

# Light Cone Cancellation for Variational Quantum Eigensolver Ansatz

Xinjian Yan,<sup>1,\*</sup> Xinwei Lee,<sup>2,†</sup> Ningyi Xie,<sup>1</sup> Yoshiyuki Saito,<sup>3</sup> Leo Kurosawa,<sup>3</sup> Nobuyoshi Asai,<sup>4</sup> Dongsheng Cai,<sup>5</sup> and Hoong Chuin LAU<sup>2</sup>

<sup>1</sup>*Graduate School of Science and Technology, University of Tsukuba*

<sup>2</sup>*School of Computing and Information Systems, Singapore Management University*

<sup>3</sup>*Graduate School of Computer Science and Engineering, University of Aizu*

<sup>4</sup>*School of Computer Science and Engineering, University of Aizu*

<sup>5</sup>*Faculty of Engineering, Information and Systems, University of Tsukuba*

Variational Quantum Algorithms (VQAs) represent a class of algorithms that utilize a hybrid approach, combining classical and quantum computing techniques. In this approach, classical computers serve as optimizers that update circuit parameters to find approximate solutions to complex problems. In this study, we apply a method known as Light Cone Cancellation (LCC) to optimize variational circuits, effectively reducing the required number of qubits and gates for circuit simulation. We then evaluate the performance of LCC on one of the VQAs—the Variational Quantum Eigensolver (VQE)—to address the Max-Cut problem. Compared with the Quantum Approximate Optimization Algorithm (QAOA), VQE offers greater degrees of freedom and promising results at lower circuit depths. By applying LCC to VQE, we can shift the complexity of circuit simulation from the number of qubits to the number of edges in the graph, i.e., from exponential time to polynomial time. This enables us to solve large problems up to 100 vertices, without actually simulating the entire circuit. From our simulation in a 7-qubit and a 27-qubit fake backends, we show that LCC yields higher approximation ratios than those cases without LCC, implying that the effect of noise is reduced when LCC is applied.

## I. INTRODUCTION

Many combinatorial optimization problems (COP) are considered to be difficult to address using traditional computational approaches. COPs aim to find the optimal combination of variables that minimizes (or maximizes) a given objective function, while simultaneously satisfying a set of constraints. Recent years, people focus on using quantum-classical hybrid methods, known as the variational quantum algorithms (VQA) [1] to heuristically solve COPs. The quantum approximate optimization algorithm (QAOA) [2] is one of the VQAs that is intensively explored due to its predictable patterns in the variational parameters [3–5], and also its relation with quantum annealing [6, 7]. Another VQA, the variational quantum eigensolver (VQE) [8], is also capable of solving COPs, while it is more known for its application to quantum chemistry. Unlike QAOA which has a problem-dependent ansatz, the structure of the VQE ansatz is static and does not depend on the problem solved. Moreover, the VQE ansatz offers a greater degree of freedom in the sense that it has greater expressibility [9] and more number of variational parameters compared to the QAOA ansatz. In our previous work, we have shown that VQE generally has better performance than QAOA and the Multi-angle QAOA [10] in solving the Max-Cut problem using noiseless simulations.

The VQAs have shown the potential quantum advantage on Noisy Intermediate Scale Quantum (NISQ) [11] devices. However, an increase in the number of qubits

often leads to higher error rates when building actual quantum hardware. Although recent advancements have prominently featured quantum error correction algorithms, it involve intricate designs that must effectively address the inherent noise and decoherence in quantum environments. It seems that reducing the number of qubits and the number of gates is a more feasible and efficient approach while maintaining the accuracy of the algorithm.

In this paper, we apply a method known as Light Cone Cancellation (LCC) [12, 13] to solve the Max-Cut problem using VQE. When computing the expectation function of variational circuits, there are many redundant operators that need not be included in the computations. LCC exploits the preliminary knowledge of which operators are redundant, so that we do not include them in the calculation at the first place. LCC is widely applied for circuits like QAOA, and also inspired the tensor network for QAOA [14–16]. The contribution of our work is that we exploit LCC on the two-local ansatz of VQE. Particularly, we design the sub-circuits for LCC-VQE and analyze its performance, supported by experimental evidences with noisy devices. To verify the impact of LCC for VQE in a noisy environment, we conduct experiments using simulated noisy backends with 7 qubits and 27 qubits. Experiments show that compared with original VQE, the implementation of LCC has better performance.

The rest of the paper is structured as follows. Section II provides background information and the construction architecture of LCC. The detailed results of experiments are articulated in Section III. Section IV contains the concluding remarks of this study.

\* yanxinjian@cavelab.cs.tsukuba.ac.jp

† xwlee@smu.edu.sg

## II. BACKGROUND

### A. Max-Cut

Max-Cut is a fundamental and widely studied NP-complete problem in the field of graph theory. The primary objective of Max-Cut is to partition the nodes of an undirected graph into two disjoint subsets such that the number of edges connecting the two subsets is maximized. This problem finds relevance in diverse fields, including network design, VLSI layout, community detection, and social network analysis[17].

Consider an  $n$ -node unweighted, undirected graph  $G = (V, E)$ , where  $V$  represents the set of the nodes and  $E$  represents the set of the edges of graph  $G$ . A cut is defined as a partition of the original set  $V$  into two subsets. The cost function  $C(\mathbf{x})$  to be maximized is the sum of the edges connecting points in the two different subsets, which can be expressed as:

$$C(\mathbf{x}) = \sum_{(i,j) \in E} (x_i \oplus x_j), \quad (1)$$

where  $\mathbf{x} = (x_1, x_2, \dots, x_n)$  and  $x_i \in \{0, 1\}$  represent the binary variable of node  $i$ . The symbol  $\oplus$  denotes the XOR (exclusive-OR) operation. We want to find the combinations of  $\mathbf{x}$  such that the cost function is maximized, which also means that make the number of edges cut is maximum. A brute-force approach in a classical computer will require an  $\mathcal{O}(2^n)$  time to solve this problem.

In the quantum realm, the cost function in Eq. (1) can be formulated as the cost Hamiltonian  $H_C$ , in which its expectation is to be maximized:

$$H_C = \frac{1}{2} \sum_{(i,j) \in E} (I - Z_i Z_j), \quad (2)$$

where  $I$  is the identity matrix of size  $2^n \times 2^n$ , and  $Z_i$  represents Pauli- $Z$  observable on qubit  $i$ . One node in the graph is mapped to one qubit in the quantum circuit, so it requires  $n$  qubits to encode the solution of Max-Cut.

### B. Variational Quantum Eigensolver

The variational quantum eigensolver (VQE) is initially developed for calculating the minimum energy states of molecules. When re-formulated to address the Max-Cut problem, the expectation value of the cost Hamiltonian  $H_C$  over a trial state  $|\psi(\boldsymbol{\theta})\rangle$  is defined as

$$E(\boldsymbol{\theta}) = \langle \psi(\boldsymbol{\theta}) | H_C | \psi(\boldsymbol{\theta}) \rangle. \quad (3)$$

The objective is to maximize  $E(\boldsymbol{\theta})$ , which is equivalent to minimizing  $-E(\boldsymbol{\theta})$ , using a classical optimizer.  $\boldsymbol{\theta}$  is the collection of variational parameters for the VQE ansatz circuit. In this paper, we employ a two-local circuit with

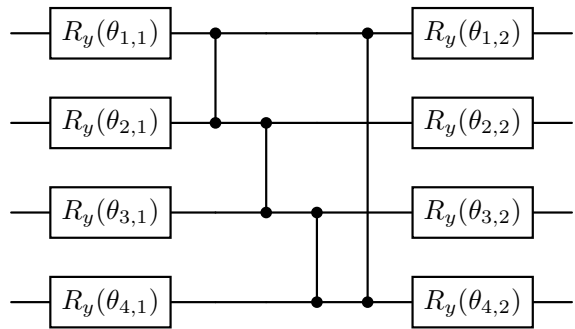


FIG. 1: Two-local ansatz used in the experiments in our work. The architecture of a single layer of  $R_y$  gates with circular CZ entanglement is used. The figure shows a 4-qubit example. The parameters  $\theta_{k,l}$  are based on the notation specified in Eq. (4).

$R_y(\theta)$  single-qubit rotation gates and CZ (controlled-Z) circular entanglement, with only a single layer. Fig. 1 shows an example of a 4-qubit ansatz circuit. The circular entanglement has CZ gates between adjacent qubits, and also between the first and the last qubit. Instead of using a flattened array  $\boldsymbol{\theta}$ , we use a matrix  $\Theta$  to represent the variational parameters to suit the geometrical position of those parameters in the circuit:

$$\Theta = \begin{bmatrix} \theta_{1,1} & \theta_{1,2} \\ \theta_{2,1} & \theta_{2,2} \\ \vdots & \vdots \\ \theta_{n,1} & \theta_{n,2} \end{bmatrix}. \quad (4)$$

It is important to note that  $\Theta$  is simply the re-shaped version of  $\boldsymbol{\theta}$ , and the notation  $\theta_{k,l}$  denotes the  $l$ -th parameter for the  $k$ -th qubit in the original circuit. Also, due to the periodicity of the  $R_y$  rotation gate, the range of the values for  $\theta_{k,l}$  are restricted to  $[0, 2\pi)$ .

Numerous metrics are available for assessing the performance of VQE. Within the scope of unconstrained COP, our focus is on studying the approximation ratio (AR). This metric compares the expected solutions obtained through VQE with that of the optimal solutions, essentially measuring the efficiency of VQE in approximating the best possible outcome. It is defined as:

$$\text{AR} = \frac{E(\boldsymbol{\theta}^*)}{\text{MaxCut}(G)}, \quad (5)$$

where  $\boldsymbol{\theta}^*$  is the quasi-optimal parameters returned by the optimizer,  $E(\boldsymbol{\theta}^*)$  is its corresponding expectation, and  $\text{MaxCut}(G)$  is the real solution of graph  $G$ . The closer the value of AR is to 1, the closer it is to the true solution of Max-Cut.

The performance of noiseless VQE and QAOA in addressing Max-Cut problems is evaluated in a previous research. When both algorithms are initialized with the same number of parameters, our findings indicate that VQE outperforms QAOA using random initialization. Furthermore, a comparison with Multi-angle quantum

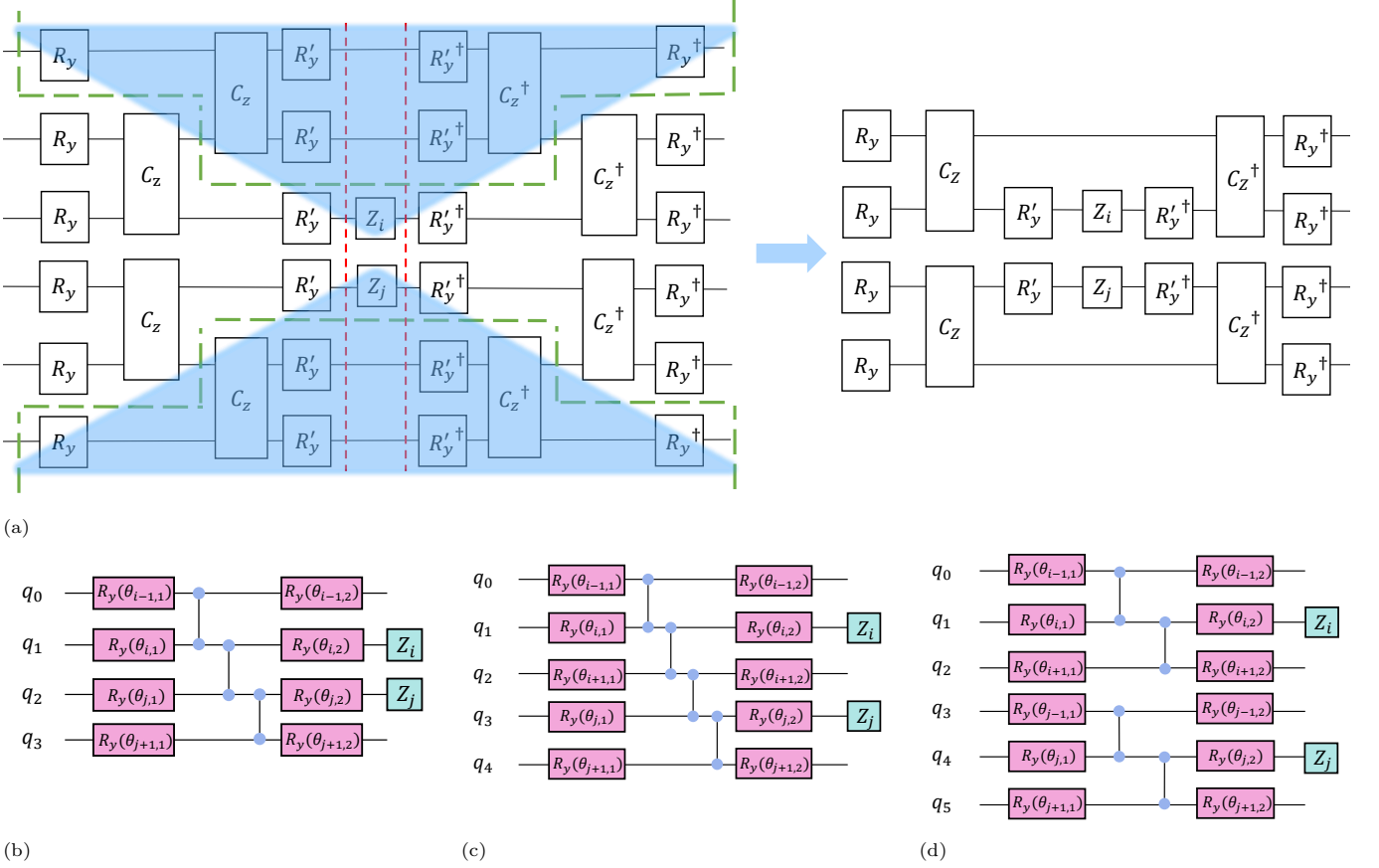


FIG. 2: (a) The light cone cancellation (LCC) in a single layer two-local ansatz. The expectation function  $\langle \psi(\theta) | Z_i Z_j | \psi(\theta) \rangle$  is visualized as a quantum circuit on the left figure.  $R_y$ 's are the single-qubit gates and  $C_Z$ 's are the two-qubit gates. The gates on the left of the red dashed line show  $|\psi(\theta)\rangle$  and the gates on the right show  $\langle \psi(\theta) |$ . The blue shaded regions show the redundant gates that can be cancelled during the calculation of the expectation. The figure on the right shows the resulting circuit after cancellation. (b), (c) and (d) shows the possible resulting circuit for the Max-cut Hamiltonian, depending on the indices  $i$  and  $j$  (positions of the Pauli-Z operators). (b) When  $Z_i$  and  $Z_j$  are adjacent; (c) when  $Z_i$  and  $Z_j$  are one qubit apart; and (d) when  $Z_i$  and  $Z_j$  are two or more qubits apart.

approximate optimization algorithm (ma-QAOA) [10] reveals that VQE also achieves superior performance in different undirected graphs [18]. The reason for this is that at the same circuit depth (same number of layers), the expressibility in VQE is greater than that in ma-QAOA, which in turn is greater than that in QAOA.

### C. Light Cone Cancellation

Light cone cancellation (LCC) is a method that utilizes the intrinsic property of the expectation function, so that the redundant unitaries in the expectation function are not included in the computation of the expectation function in the first place [19]. The LCC property was originally used in QAOA in reducing the problem graphs into their constituent subgraphs, hence simplifying the problem to be solved [20–22]. It also inspired applications like the tensor network of QAOA [14–16].

Referring to Eq. (2), for a Hamiltonian  $H_C$  that can be written as the sum of local observables, the trial wave-

function (or ansatz) of both sides,  $\langle \psi(\theta) |$  and  $|\psi(\theta)\rangle$ , can be cancelled out partially. This is because some of the unitary gates used to prepare  $|\psi(\theta)\rangle$  commutes through the central local observables. Fig. 2(a) shows an example of the LCC of a two-local circuit used to prepare the trial wavefunction for VQE. The figure visualizes the expectation function Eq. (3) as a quantum circuit. The circuit on the left of the red dashed line shows the term  $|\psi(\theta)\rangle$ , and the circuit on the right of the dashed line shows  $\langle \psi(\theta) |$ , with the central observable  $Z_i Z_j$  (between the red dashed lines) acting on qubit  $i$  and  $j$ . Since  $|\psi(\theta)\rangle$  is just the conjugate transpose of  $\langle \psi(\theta) |$ , they are the counterpart of each other in the circuit. The blue shades show the gates that are not related to qubits  $i$  and  $j$  can commute through the center and are cancelled. The result of the cancellation is shown on the right of Fig. 2(a), which has reduced the number of qubits and number of gates.

The Max-Cut Hamiltonian in Eq. (2) has a two-local  $Z$  observable on every term. After LCC on the two-local ansatz that we considered (single layer  $R_y$  and circular CZ entanglement), we can get 3 different types of sub-

circuits as shown in Fig. 2(b), (c) and (d), which requires a 4-, 5-, and 6-qubit quantum circuit, respectively. Circular entanglement means the adjacent qubits, as well as the first and the last qubits, are entangled. Note that one sub-circuit corresponds to the expectation of a local term in the Hamiltonian, so the simulation of the sub-circuits can be done separately. Also, the sub-circuit in Fig. 2(d) can be further divided into two separate circuits as the first 3 qubits and the last 3 qubits are not entangled. Thus, we only require a maximum of 5 qubits to simulate the expectation of the entire Max-Cut Hamiltonian, regardless of the problem size. In fact, the maximum number of qubits,

$$n_q = 2k + 1, \quad (6)$$

are required to simulate the expectation of a Hamiltonian with  $k$ -local observables, for this kind of ansatz (one layer of single-qubit gates and circular entanglement). The architecture of the entanglement is crucial in deciding how many qubits we can reduce. For linear entanglement (adjacent qubits entangled, first and last not entangled), there would be another case of the sub-circuits where the observable is located on the first qubit or on the last qubit. For full entanglement (all qubits entangled), LCC will not be possible.

Since now the number of qubits required stays constant, the complexity of circuit simulation now shifts to the number of sub-circuits, i.e. the number of terms that is in the Hamiltonian. For Max-Cut, the number of terms scales with the number of edges in the graphs, which is at most  $n(n-1)/2$  edges (a complete graph). Without LCC, the simulation complexity would be dominated by the number of qubits  $n$ , which takes  $\mathcal{O}(2^n)$  space and time when simulated classically. With LCC, the time complexity now depends on the number of edges of the graph, which is  $\mathcal{O}(n^2)$ . The shift in complexity of quantum circuit simulation, from exponential to polynomial, is a significant advantage for LCC.

Another advantage for LCC is that the number of gates is reduced, which in turn reduces the effect of gate noises in quantum devices. On the other hand, it is also worth noting that even though the number of qubits and the number of gates are reduced, the number of parameters stays unchanged after LCC. This is because the sub-circuits after LCC will have different parameters corresponding to the indices  $i$  and  $j$ , depending on where the observables  $Z_i Z_j$  are. For example, referring to the sub-circuit in Fig. 2(b), the  $Z_2 Z_3$  term associates with the parameters

$$\begin{bmatrix} \theta_{1,1} & \theta_{1,2} \\ \theta_{2,1} & \theta_{2,2} \\ \theta_{3,1} & \theta_{3,2} \\ \theta_{4,1} & \theta_{4,2} \end{bmatrix}$$

in the sub-circuit, while the term  $Z_5 Z_6$  associates with

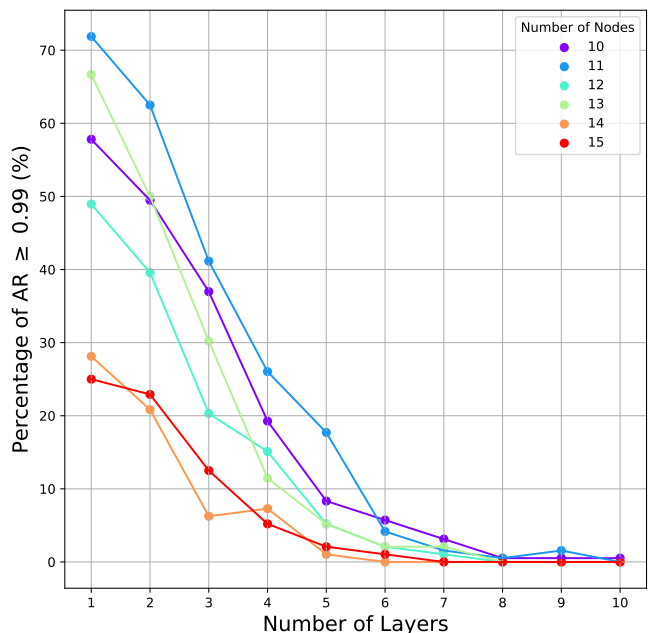


FIG. 3: Percentage of AR  $\geq 0.99$  in different number of layers of the ansatz. For  $n = 10, 11, 12$ , each point shows the percentage calculated from 8 graph instances, each with 24 different random initial parameters, with a total of 192 trials. For  $n = 13, 14, 15$ , each point shows the percentage for 4 graph instances, each with 24 trials, with a total of 96 trials. Each trial represents a set of random initial parameters, converged to the given AR after an optimization run.

different parameters

$$\begin{bmatrix} \theta_{4,1} & \theta_{4,2} \\ \theta_{5,1} & \theta_{5,2} \\ \theta_{6,1} & \theta_{6,2} \\ \theta_{7,1} & \theta_{7,2} \end{bmatrix}.$$

Therefore, the difficulty in optimization remains the same before and after LCC.

LCC is also applicable for other circuits like QAOA and ma-QAOA. However, QAOA or ma-QAOA usually needs more layers (larger circuit depths) to achieve higher ARs. Meanwhile, VQE with even one layer is enough to reach most of the states and hence easier to reach higher ARs than QAOA. This is due to the difference in expressibility between the VQE ansatz and the QAOA ansatz [9]. Since VQE yields higher ARs with fewer layers than QAOA, LCC-VQE can be done with fewer qubits, compared to LCC-QAOA or LCC-ma-QAOA.

#### D. Number of layers in the ansatz

In this work, we only consider a single layer of the VQE ansatz as it is sufficient to address the Max-Cut problem. To justify this, we conducted an experiment to investigate the variation of the quality of the solution to the number of layers of the two-local ansatz. Fig. 3 shows

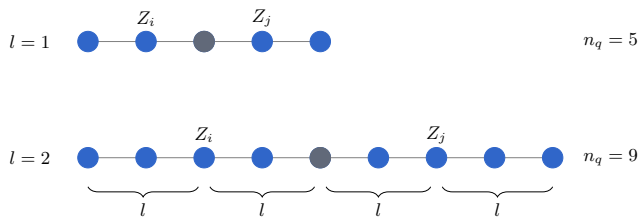


FIG. 4: The entanglement map after LCC when the number of ansatz layers increases. Each node represents a qubit and each edge represents an entanglement. The figure shows the maximum number of qubits required for the linear or circular entanglement after LCC. The number of qubits required for LCC also depends on the number of qubits of the original ansatz, and also the distance between the observables. The maximum number of qubits is achieved when the observables are exactly  $2l$  qubits apart of each other. To achieve maximum number of qubits, each of the observables stretches out a distance of  $l$  qubits (blue nodes) for two sides, and they overlap at the grey node, forming an inseparable entanglement.

that, as the number of layers increases, the chance of obtaining a high-quality solution ( $\text{AR} \geq 0.99$ ) decreases. The chance of obtaining a high-quality solution is quantified by the percentage, i.e., the total number of times  $\text{AR} \geq 0.99$  obtained, divided by the total number of trials. For  $n = 10, 11, 12$ , each point shows the percentage calculated from 8 graph instances, each with 24 different random initial parameters, with a grand total of  $8 \times 24 = 192$  trials. For  $n = 13, 14, 15$ , each point shows the percentage for 4 graph instances, each with 24 trials, with a total of 96 trials. The decline in the percentage can be explained by the increasing difficulty of optimization as the number of layers (number of parameters) increases, possibly the increased number of local minima, causing overparameterization where the AR could not increase further despite increasing the number of parameters. Hence, we justify that the ansatz of a single layer is sufficient for the problem instances considered.

Let us consider what happens to LCC when we have more than one layer of the ansatz. As the number of layers increases, the number of gates that can be cancelled decreases, resulting in a larger sub-circuit after LCC. This is because entangling gates (CZ gate in our case) farther from the center cannot commute through the layers nearer to the center (where the observables are) to get cancelled out on the other side, causing them to remain in the circuit after LCC (refer to Fig. 2, where the area outside the light cone gets larger if the circuit has more layers). The number of qubits remaining after LCC depends on the entanglement structure of the ansatz. The entanglement map of a quantum circuit can be viewed as a graph with the qubits as the nodes and the entanglement as the edges, e.g., if there is an entangling gate between qubit  $i$  and qubit  $j$ , then there is an edge between node  $i$  and node  $j$ . The resulting entanglement map, after LCC, can then be viewed as a subgraph spanned by the observables  $Z_i$  and  $Z_j$ , from the distance  $l$

nodes away from node  $i$  and node  $j$ , where  $l$  is the number of layers in the original ansatz. This is analogous to the idea where QAOA is said to search deeper subgraphs as its circuit depth  $p$  increases [2, 20, 23]. Fig. 4 shows the visualization of the entanglement map after LCC, considering the largest subgraph that can be spanned by the two observables. For linear and circular entanglement, the subgraphs are represented by line graphs. To calculate the maximum number of qubits required after LCC, we consider the case where the size of the subgraph is at its maximum. This happens when the observable nodes stretch out for a distance  $l$  to each side and overlap at their ends, similar to the sub-circuit in Fig. 2(c) in the case of  $l = 1$ . The grey nodes in Fig. 4 show the overlapping nodes for each observable. Thus, it is not difficult to establish a relation between the maximum number of qubits required  $n_q$  with the number of layers  $l$ :

$$n_q = 4l + 1, \quad (7)$$

for 2-local observables like the Max-Cut Hamiltonian. For  $k$ -local observables, the maximum number of qubits is

$$n_q = 2kl + 1. \quad (8)$$

Note that  $n_q$  is the maximal case where  $n \geq n_q$  and the observables are exactly  $2l$  qubits apart from each other. The maximum number of qubits required will still be bounded by the original graph size  $n$ , and also when the observables are nearer or farther from each other. Eq. (6) and (7) are the special cases for Eq. (8) when  $l = 1$  and  $k = 2$  respectively, in the case where the ansatz only has one layer, or the observables are 2-local.

### III. RESULTS

We solve the Max-Cut problem using VQE with a two-local ansatz (single layer  $R_y$  and CZ entanglement), and we use the COBYLA optimizer [24] for all the experiments. The experiments are to compare the performances of the VQE with LCC and that without LCC. We measure the performance using the approximation ratio (AR), which defines how near the result given by VQE is to the actual solution. To make sure that the optimizer does not converge to a good minimum by chance, we perform 24 trials of random initial parameters for every instance, i.e., random initialization. The experiments are performed under noisy conditions so that we can observe the effect of the reduction in the number of qubits and the number of gates on the amount of noise in the circuit. We use two different fake noisy devices provided by Qiskit [25]: *FakeCasablanca* (7 qubits) and *FakeParis* (27 qubits). The fake devices simulate the same noise settings in their respective real quantum devices.

Figure 5 shows the comparison between Max-Cut instances solved with LCC on the 7-qubit fake backend,

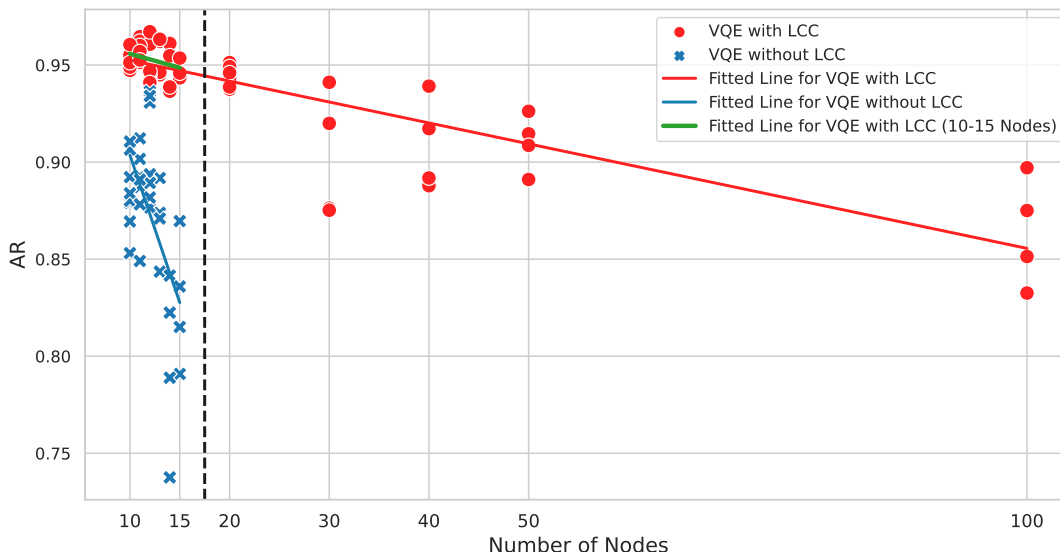


FIG. 5: Comparison of the approximation ratio (AR) for the VQE solved with a 7-qubit fake backend **FakeCasablanca** (with LCC) and a 27-qubit fake backend **FakeParis** (without LCC). Each point shows the best AR (highest) chosen out of 24 trials. The lines are linear fits of their respective data. Meanwhile, the gradients of the red line, blue line, and green line are  $-0.0011$ ,  $-0.0152$  and  $-0.0018$ , respectively.

and those solved without LCC on the 27-qubit fake backend. As only 5 qubits are required to simulate the subcircuits for LCC, the VQE simulation can be run on a device with 7 qubits. On the other hand, simulation with full number of qubits is required for those without LCC. In both settings, we solve the Max-Cut for 36 non-isomorphic instances, ranging from number of vertices  $n = 10$  to  $n = 15$ . Additionally, 24 non-isomorphic instances are solved on the 7-qubit fake backend (with LCC) for  $n = 20, 30, 40, 50$  and  $100$ . The dataset for the experiments is shown in the Appendix. Each point in the plot represents the best AR out of 24 trials for a single problem instance. The red points plot the ARs for the instances solved with LCC on the 7-qubit fake backend; the blue points plot the ARs for the instances solved without LCC on the 27-qubit fake backend. The red line is a linear fit through the red points (with LCC) for  $n = 10$  to  $n = 100$ . The blue line linearly fits through the blue points (without LCC) for  $n = 10$  to  $n = 15$ . The green line is a fit for the red points (with LCC) from  $n = 10$  to  $n = 15$ .

There are a few observations worth noting. LCC enabled the simulation of large problems up until  $n = 100$ , only with quantum circuits with at most 5 qubits. From the red and blue fitted lines, we can see that the ARs for problems with LCC are generally higher than those without LCC. Although with different environments (7-qubit and 27-qubit fake backends), the error rate is generally lower on a smaller device, so the AR is not so much deteriorated on a 7-qubit device. Moreover, with less number of gates, the effect of noise on the AR is also reduced. It can also be observed that the AR decreases as the problem size (number of vertices of the graph) increases. Another interesting point to note is that the green line has

similar slope as the red line, which means the decreasing trend is similar for microscopic ( $n = 10$  to  $n = 15$ ) and macroscopic ( $n = 10$  to  $n = 100$ ) number of nodes. Also, we can observe from the blue line that if without LCC, the AR decreases faster due to more noises in the circuits. This implies the possibility that in the case without LCC, the AR would decrease faster than the case with LCC, if the blue line is extrapolated to larger problem size.

Figure 6 shows the comparison for  $n = 10$  to  $n = 15$  problems solved with and without LCC, using the same 27-qubit backend. The 36 instances used are the same as those in Fig. 5. The diagonal dashed line shows where both methods (with and without LCC) have the same AR. All the points are in the lower triangle which represent that LCC gives higher ARs than without having LCC. Under the same noise conditions, it can be observed that all the 36 instances give higher ARs with LCC applied. This result shows the effect of the reduction in the number of gates in a more evident way than the experiment shown in Fig. 5, as the number of qubits and the error rates are the same for both with and without LCC. It is also observed that problems with larger size  $n$  benefit more from LCC as their ARs stay away from the diagonal dash line, and those with smaller sizes stay near the diagonal dash line. This is because larger circuits generally have more noise, causing their ARs to deteriorate more.

#### IV. CONCLUSION

In this work, we presented the LCC on VQE and studied what the effect it acts in solving the Max-Cut problem. Our work opens up the possibility of using VQE to

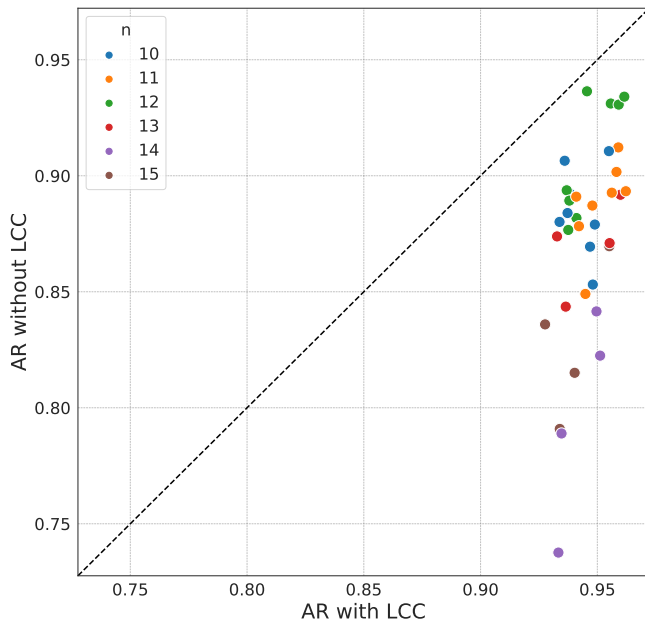


FIG. 6: Comparison of the AR for the VQE with LCC and without LCC, using the same FakeParis backend (27 qubits). The diagonal dashed line shows where the AR of both methods are equal. All the points are in the lower triangle and represent higher AR with LCC.

solve combinatorial optimization problems, as VQE requires less number of layers than QAOA to achieve the same performance. This allows us to cancel a larger number of qubits when applying LCC, thereby shifting the complexity of circuit simulation from exponential scaling (number of qubits) to polynomial scaling (number of edges in a graph). For the Max-Cut problem with a two-local cost Hamiltonian, only at most five qubits are required to solve the problem of any size. Concerning the implementation of LCC, our preliminary calculations reveal the relationship between the maximum number of qubits  $n_q$  with  $k$ -local observables in calculating the expectation of Hamiltonian  $H_C$ . It is worth noting that LCC can only be implemented under linear and circular entanglement structures, whereas it is not feasible under full entanglement. To look at the precise relation between high-quality solution and layer numbers in addressing Max-Cut problem, we compare the performance of VQE ansatz with different number of layers and conclude that the opportunity to achieve a high-quality solution ( $AR \geq 0.99$ ) comes to decrease with the number of layers  $l$  increases. This decline is attributed to tendency to become trapped in local minimas due to overparameterization. Meanwhile, the computational cost increases with the number of layers  $l$ , and those causes make it necessary for the optimization process to achieve faster convergence rate by setting the ansatz to a single layer. Furthermore, as the number of layers  $l$  increases, the size of sub-circuits with the maximum number of qubits  $n_q = 4l + 1$  also grows. This can significantly undermine the effectiveness of LCC in a noisy environment.

We compare the performance of circuits with and without LCC on a noisy simulator provided by Qiskit. The results show that the circuits with LCC generally yield higher approximation ratios than the circuits without LCC, hence implying that the noise is being mitigated. As presented in the previous sections, it is unclear whether the LCC could lead to a quantum advantage for VQE in a lower layer with circular entanglement. To overcome those challenges, one direction is to conduct more comprehensive and in-depth experiments. It would be fruitful to pursue further research about combining LCC with other algorithms in order to reduce circuit's noise. Additionally, due to its advantages with fewer layers, LCC-VQE is hoped to be tested on other combinatorial optimization problems. It could become an interesting and valuable development for helping VQA mitigate the effects of noise.

### Appendix A: Dataset of the experiments

Table I shows the experiment datasets we conducted in this study, we use two categories of unweighted, undirected graphs: the  $G(n, p)$  Erdős-Rényi graphs and the regular graphs. The graphs are generated using the NetworkX Python package. The  $G(n, p)$  graphs are generated using `fast_gnp_random_graph()`; the regular graphs are generated using `random_regular_graph()`, with the seeds specified. Each seed represents one graph instance.

### Appendix B: Noise Model for Fake Backends

Table II shows the detailed noise models for the two fake backends used in our simulations: FakeCasablanca (7 qubits) and FakeParis (27 qubits). The basis gates for the two fake devices are the  $X$ ,  $\sqrt{X}$ ,  $R_z$  (rotational  $Z$  gate) and the CNOT gate. The  $R_z$  gates have zero error and the errors for the rest of the gates are stated in the table. The ansatzes will be decomposed to the basis gates before being executed in the fake devices.  $T_1$  and  $T_2$  are the average relaxation and dephasing times.

TABLE I: The datasets used in the experiments—the regular graphs with degree  $d$  and  $G(n, p)$  graphs with edge probability  $p$ .

No. of nodes	Graph type	$d$ (Reg.) or $p$ (ER)	Seed
10	ER	0.5	0, 1, 2, 3
10	Reg.	3	0, 1, 2, 3
11	ER	0.5	0, 1, 2, 3
11	Reg.	4	0, 1, 2, 3
12	ER	0.5	0, 1, 2, 3
12	Reg.	3	0, 1, 2, 3
13	ER	0.5	0, 1
13	Reg.	2	1, 3
14	ER	0.4	0, 1
14	Reg.	2	2, 5
15	ER	0.3	1, 2
15	Reg.	2	3, 7
20	ER	0.25	0, 3, 5, 17
20	Reg.	3	0, 1, 2, 3
30	ER	0.12	0, 5
30	Reg.	2	3, 8
40	ER	0.06	106, 125
40	Reg.	2	0, 1
50	ER	0.06	126, 167, 424, 561
100	ER	0.035	86520, 769454
100	Reg.	3	0, 1

TABLE II: Noise model for the fake backends.

	FakeCasablanca	FakeParis
$X$ and $\sqrt{X}$ gate errors	$4.63 \times 10^{-4}$	$4.34 \times 10^{-4}$
CNOT gate errors	$1.29 \times 10^{-2}$	$1.30 \times 10^{-2}$
Readout errors	$1.74 \times 10^{-2}$	$1.78 \times 10^{-2}$
$T_1$ ( $\mu s$ )	88.06	82.70
$T_2$ ( $\mu s$ )	77.27	77.22

- 
- [1] M. Cerezo, A. Arrasmith, R. Babbush, S. C. Benjamin, S. Endo, K. Fujii, J. R. McClean, K. Mitarai, X. Yuan, L. Cincio, *et al.*, *Nature Reviews Physics* **3**, 625 (2021).
- [2] E. Farhi, J. Goldstone, and S. Gutmann, arXiv preprint arXiv:1411.4028 (2014), arXiv:arXiv:1411.4028 [quant-ph].
- [3] L. Zhou, S.-T. Wang, S. Choi, H. Pichler, and M. D. Lukin, *Phys. Rev. X* **10**, 021067 (2020).
- [4] J. Cook, S. Eidenbenz, and A. Bäertschi, 2020 IEEE International Conference on Quantum Computing and Engineering (QCE), 83 (2020).
- [5] X. Lee, N. Xie, D. Cai, Y. Saito, and N. Asai, *Mathematics* **11**, 2176 (2023).
- [6] E. Farhi, J. Goldstone, S. Gutmann, and M. Sipser, arXiv preprint arXiv:quant-ph/0001106 (2000), arXiv:arXiv:quant-ph/0001106.
- [7] S. H. Sack and M. Serbyn, *Quantum* **5**, 491 (2021).
- [8] A. Peruzzo, J. McClean, P. Shadbolt, M.-H. Yung, X.-Q. Zhou, P. J. Love, A. Aspuru-Guzik, and J. L. O’Brien, *Nature communications* **5**, 4213 (2014).
- [9] S. Sim, P. D. Johnson, and A. Aspuru-Guzik, *Advanced Quantum Technologies* **2**, 10.1002/qute.201900070 (2019).
- [10] R. Herrman, P. C. Lotshaw, J. Ostrowski, T. S. Humble, and G. Siopsis, Multi-angle quantum approximate optimization algorithm (2021), arXiv:2109.11455 [quant-ph].
- [11] J. Preskill, *Quantum* **2**, 79 (2018).
- [12] A. Lowe, M. H. Gordon, P. Czarnik, A. Arrasmith, P. J. Coles, and L. Cincio, *Physical Review Research* **3**, 10.1103/physrevresearch.3.033098 (2021).
- [13] L. Leone, S. F. E. Oliviero, L. Cincio, and M. Cerezo, On the practical usefulness of the hardware efficient ansatz (2022), arXiv:2211.01477 [quant-ph].
- [14] C. Huang, F. Zhang, M. Newman, X. Ni, D. Ding, J. Cai, X. Gao, T. Wang, F. Wu, G. Zhang, H.-S. Ku, Z. Tian, J. Wu, H. Xu, H. Yu, B. Yuan, M. Szegedy, Y. Shi, H.-H. Zhao, C. Deng, and J. Chen, *Nature Computational Science* **1**, 578 (2021).
- [15] D. Lykov, R. Schutski, A. Galda, V. Vinokur, and Y. Alexeev, in *2022 IEEE International Conference on Quantum Computing and Engineering (QCE)* (2022) pp. 582–593.
- [16] D. Lykov and Y. Alexeev, in *2021 IEEE Computer Society Annual Symposium on VLSI (ISVLSI)* (2021) pp. 447–452.
- [17] A. Jagannath, J. Ko, and S. Sen, *The Annals of Applied Probability* **28**, 1536 (2018).
- [18] X. Yan, X. Lee, D. Cai, and N. Asai, *IPSIJ SIG Technical Report* **2024-QS-11**, 1 (2024).
- [19] M. Benedetti, M. Fiorentini, and M. Lubasch, *Physical Review Research* **3**, 033083 (2021).
- [20] F. G. S. L. Brandao, M. Broughton, E. Farhi, S. Gutmann, and H. Neven, arXiv preprint arXiv:1812.04170 (2018), arXiv:arXiv:1812.04170 [quant-ph].



- [21] J. Basso, E. Farhi, K. Marwaha, B. Villalonga, and L. Zhou (Schloss Dagstuhl - Leibniz-Zentrum für Informatik, 2022).
- [22] J. Wurtz and D. Lykov, *Phys. Rev. A* **104**, 052419 (2021).
- [23] A. Galda, X. Liu, D. Lykov, Y. Alexeev, and I. Safro, Transferability of optimal qaoa parameters between random graphs (2021), arXiv:2106.07531 [quant-ph].
- [24] M. J. D. Powell, A direct search optimization method that models the objective and constraint functions by linear interpolation, in *Advances in Optimization and Numerical Analysis* (1994) pp. 51–67.
- [25] Qiskit contributors, Qiskit: An open-source framework for quantum computing (2023).